GSA Data Repository 2020125

Reconstructing Tonian seawater $^{87}Sr/^{86}Sr$ using calcite microspar

Ying Zhou[1], Philip A.E. Pogge von Strandmann[1], Maoyan Zhu[2,3], Hongfei Ling[4], Christina Manning[5], Da Li[4], Tianchen He[6] and Graham A. Shields[1]

[1] London Geochemistry and Isotope Centre, Institute of Earth and Planetary Sciences, University College London and Birkbeck, University of London, Gower Street, London, WC1E 6BT, UK

[2] State Key Laboratory of Palaeobiology and Stratigraphy and Center for Excellence in Life and Paleoenvironment, Nanjing Institute of Geology and Palaeontology, Chinese Academy of Sciences, Nanjing 210008, China

[3]College of Earth and Planetary Sciences, University of Chinese Academy of Sciences, Beijing 100049, China

[4]School of Earth Sciences, Nanjing University, Nanjing, 210023

[5]Department of Earth Sciences, Royal Holloway, University of London, Egham, TW20 0EX

[6]School of Earth and Environment, University of Leeds, Leeds, LS2 9JT

SUPPLEMENTARY INFORMATION

Detailed geological background

Modern China is composed of three major cratons: South China, North China and Tarim, all of which retain a record of Neoproterozoic rifting events that have been linked to the break-up of the supercontinent Rodinia (Li et al., 1996). The North China Craton (NCC), also known as the Sino-Korean Craton, has an Archean to Paleoproterozoic basement and well-developed Mesoproterozoic to Neoproterozoic sedimentary cover. To the South it is bordered by the Dabie-Sulu orogenic belt and to the North by the Central Asian orogenic belt (Wang and Qiao, 1984; Li et al., 1996). The thick Neoproterozoic carbonate successions on the NCC were deposited in a shallow marine environment and have not been subjected to regional metamorphism. From the Mesoproterozoic to the Early Paleozoic, platform carbonates dominated deposition over the NCC (Yang et al., 2012), consistent with its reportedly tropical latitude in paleogeographic reconstructions (Fu et al., 2015). The thickest Neoproterozoic strata are located in the Jiao-Liao-Xu-Huai realm (Jiao: Shandong; Liao: Liaoning; Xu: Xuzhou; Huai: Huai River = Huaibei and Huainan regions), all of which lie either side of the N-S trending Tanlu strike-slip fault (Fig. S1). The Huaibei region, the main subject of the present study, can be found on the southern margin of this eastern NCC block (orange box in Fig. S1).

The best known Tonian successions of the Jiao-Liao-Xu-Huai stratigraphic realm are the Huaibei Group in the Huaibei area near Xuzhou, the Huainan Group in the Huainan area of southern Anhui, the Jinxian Group in the Dalian area and the more truncated, type locality of the Tonian (Qingbaikouan) System near Jixian (Zhang et al., 2000). Across North China, the Tonian System exhibits a characteristic sequence of lithologies, with coarse siliciclastic sediments at the base, succeeded by mudstone, and finally carbonate of varying thickness. This tripartite

succession is overlain either by glaciogenic deposits and/or evaporite facies of likely Ediacaran-Cambrian age (He et al., 2016; Wan et al., 2019). Geologists correlate the different groups that comprise the Tonian System using scarce marker beds, such as the distinctive red stromatolites of the Weiji Formation (Huaibei Group) and Shisanlitai Formation (Jinxian Group). Detrital zircon and intrusive diabase zircon and baddeleyite U-Pb ages show an early Neoproterozoic (c. 1000 Ma – c. 720 Ma) for these thick carbonate successions of the Jiao-Liao-Xu-Huai stratigraphic realm (Liu et al., 2006; Gao et al., 2009, 2010; Yang et al., 2012; Wang, Yang, et al., 2012). Although the age of the youngest portion remained largely unconstrained until recently (Zhang et al., 2016; Zhu et al., 2019), the Tonian age is also supported by biostratigraphic studies (Dong et al., 2008; Xiao et al., 2014) and in particular by the presence of the age diagnostic index acritarch, *Trachyhystrichosphaera aimika*, in both Huaibei and Huainan areas of the NCC (Tang et al., 2013, 2015). Hitherto, only few chemostratigraphic studies on these strata have been carried out, revealing that most $\delta^{13}C_{carb}$ values fall between 0‰ and +5‰ (Zang and Walter, 1992; Yang et al., 2001; Zheng et al., 2004; Xiao et al., 2014). Even fewer $^{87}Sr/^{86}Sr$ data have been published, with ratios ranging widely between 0.7055 to 0.7096 in isolated studies across the craton (Fairchild et al., 2000; Yang et al., 2001; Kuang et al., 2011; Xiao et al., 2014). The lowermost of these values are also consistent with a Tonian age (cf. Cox et al., 2016; Kuznetsov et al., 2017).

Our published detrital zircon ages reported in He et al. (2016) indicate that the topmost unit of the Huaibei Group, the Gouhou Formation, is at least partly of Cambrian age (~518 Ma). Detrital zircons of Cambrian age were confirmed in a more recent study (Wan et al., 2019) (Figure 1), which concluded that only the reddish, evaporitic and carbonate-rich upper portion of the Gouhou Formation was of Cambrian age, while lower units at Gouhou locality bear

characteristic Tonian-age fossil assemblages. A discordant hiatus of 150 to 300 million years was thus recognized between the evaporitic upper Gouhou and underlying Tonian strata.

The maximum age of the uppermost carbonate units of Huaibei Group can be estimated by correlation with the uppermost Jinxian Group, the Xingmincun Formation, which contains a youngest zircon population dated at 924 Ma ± 25 Ma (Yang et al., 2012) and is intruded by multiple diabase dykes and sills (Liu et al., 2006; Wang, Zhou, et al., 2012). At Jinxian, internally consistent results (Zhang et al., 2016) strongly indicate a co-magmatic origin for baddelyite crystals, which provide a minimum depositional age constraint of ~924 ± 5 Ma for the Xingmincun Fm and underlying Cuijiatun Fm of the Jinxian Group and 913 ± 10 Ma for the Wangshan Fm and underlying Shijia Fm of the Huaibei Group (Zhu et al., 2019). Within uncertainty, these new ages are the same as that for the oldest zircons found in intrusions of the Huaibei Group (Fu et al., 2015; Wang, Yang, et al., 2012). These 920-900 Ma dykes (sills) swarms intruded along the southeastern margin of the NCC and were named the Dashigou-CDS large igneous province or LIP (Peng et al., 2011).

All published age constraints are therefore consistent with a robust depositional age for the topmost strata of the Huaibei and Jinxian groups of ~0.92 Ga. The similarity in intrusion ages across the NCC (including Korean peninsula) imply that widespread crustal extension and related magmatism occurred shortly after cessation of deposition at Jinxian, possibly due to pre-magmatic regional uplift after ~0.92 Ga (Zhang et al., 2016). Based on all available geochronological data, deposition of these strata ranged between ~1000 Ma and ~920 Ma, as the lower formations below both groups were deposited ~1060 Ma (Fig. 1) (Yang et al., 2012). An approximate 60 million-year duration was derived from an independent analysis based on the measured rate of change of seawater $^{87}Sr/^{86}Sr$ through the Huaibei Group (see below and Fig.

S5). For the purposes of this study, it was considered therefore that the carbonate rocks of the Tonian carbonate rocks of the Huaibei and Dalian areas were deposited from 980 Ma until 920 Ma.

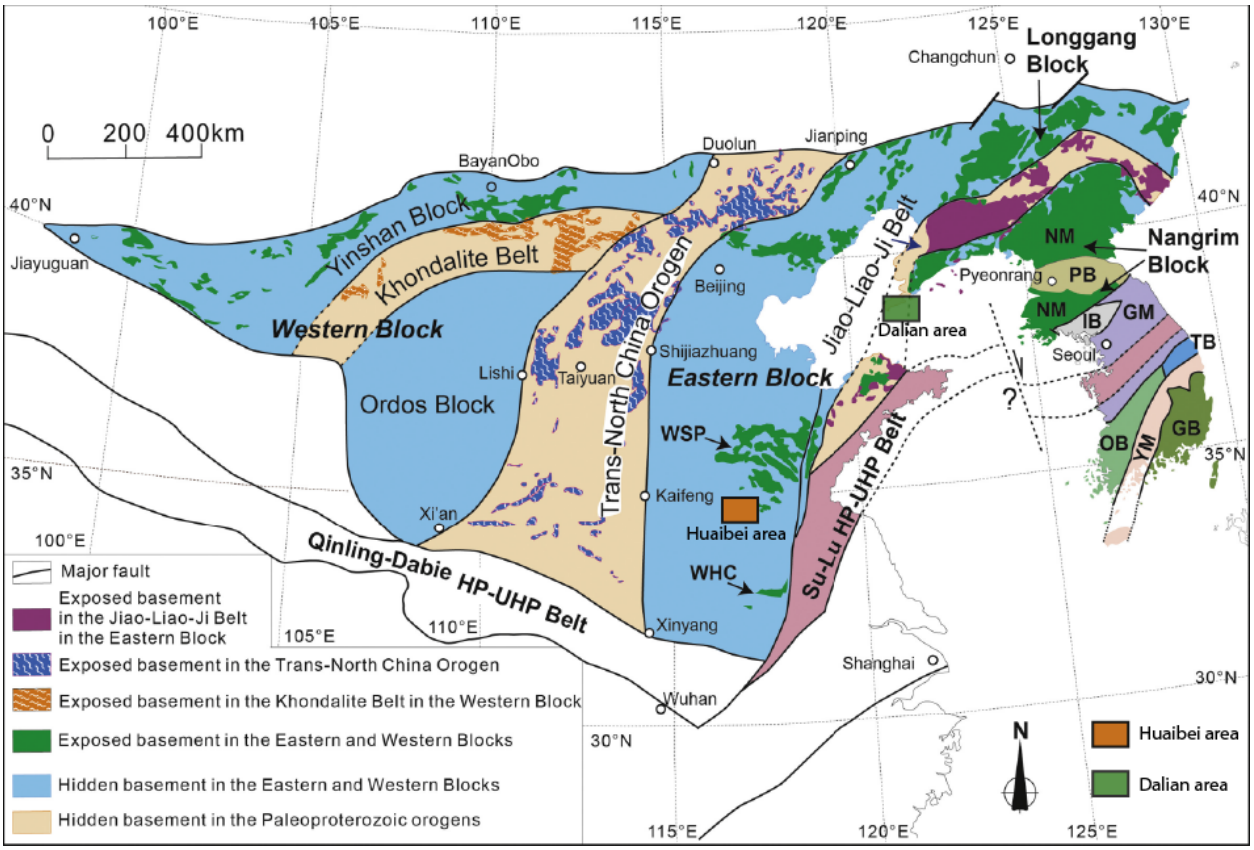

Figure S1. Three-fold tectonic subdivision of the North China Craton (Zhao et al., 2005; Zhao and Guo, 2012), map modified from Liu et al. (2017). The main field areas are located on the eastern block. Dalian area in the north (marked by the green box), and Huaibei in the south (marked by the orange box) either side of the N-S striking Tan Lu strike-slip fault.

Sampling localities in the Huaibei region

Longshan Section (LS samples): 33.90527778°N; 117.64694444° E. The section covers the top of Niyuan, Jiudingshan and Zhangqu formations and the base of Weiji Formation.

Pingshancun Section (WS samples): 33.99472222°N; 117.31638889° E. The section covers the upper part of Wangshan Formation and the Jinshanzhai Formation.

Jinshanzhai Section (JSZ samples): 33.91583333°N; 117.28444444°E. The section covers the top of Wangshan, plus Jinshanzhai and Gouhou formations.

Zhaowei Section (ZW and JY samples): 34.91194444°N; 117.48888889°E. The section covers the upper part of Jiayuan formation and Zhaowei and Niyuan formations, but samples only collected from upper Jiayuan and basal Zhaowei formations.

Yinjiazhai Section (YSZ samples): 33.91194444°N; 117.52722222°E. The section covers Weiji Formation.

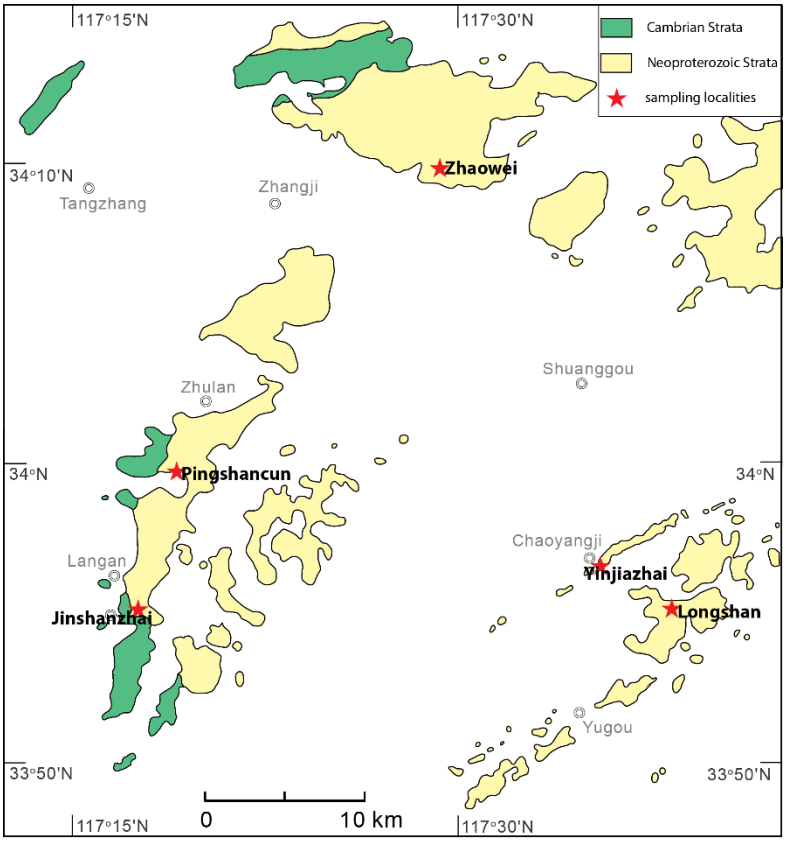

Figure S2. Huaibei Group sampling localities shown on the geological map of the Huaibei area.

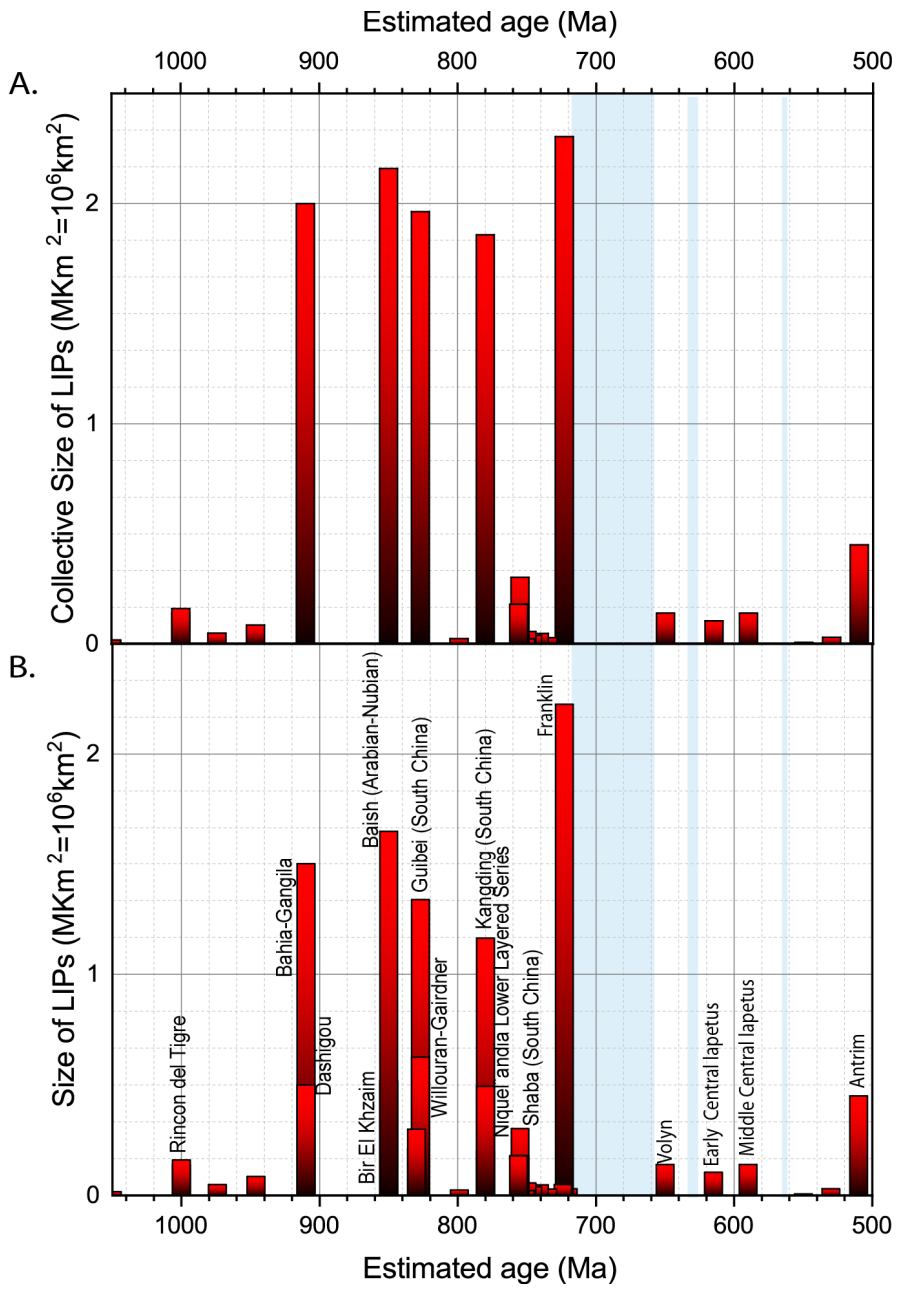

Figure S3: An updated compilation of Large Igneous Provinces from 1125 – 500 Ma based on (Ernst et al., 2008) and an updated compilation at http://www.largeigneousprovinces.org/. Additionally, the sizes of the ~920 Ma Dashigou LIP and the Bahia – Ganila LIP were updated from Peng et al. (2011) and Chaves et al. (2018). The light blue columns in the background mark the three known glaciations, from old to young: Sturtian, Marinoan and Gaskiers. A shows

the collective sizes of the LIPs with the same age; B shows the sizes and names of individual LIPs.

Petrographic and geochemical criteria used in sample selection

Petrographic criteria are commonly applied in order to distinguish primary from secondary carbonate components (Montanez et al., 1996): (1) Minimal amounts of secondary calcite that typify late-diagenetic mobilization and precipitation, e.g. veining; (2) no or low levels of recrystallization or destructive fabrics characterized by coarser grains; (3) calcitic composition; and (4) negligible secondary microporosity. The same criteria were applied carefully for the two types of sub-samples: bulk matrix and calcitic microspar cements (CMC). These early diagenetic cements have an extremely homogeneous grain size (5-15 μm) and mineralogy, compared with the surrounding matrix, even in rare cases where both can be classified as low-Mg calcite microspar. The borders of the crack-filling cements (example see Fig. S4) are usually sharp but irregular, with no evidence for secondary calcite recrystallization or dolomitisation. This is taken to demonstrate that the structure represents the infilling of an existing crack or cavity, which cemented rapidly, before lithification of the surrounding rock matrix (Pope et al., 2003; Pollock et al., 2006). Such early diagenetic, blocky microspar cements have been reported globally from carbonate rocks of Proterozoic age from ~1.9 Ga to ~0.73 Ga (Shields, 2002; Shen et al., 2016; Hodgskiss et al., 2018) with one instance of Neoarchean CMC (Bishop et al., 2006).

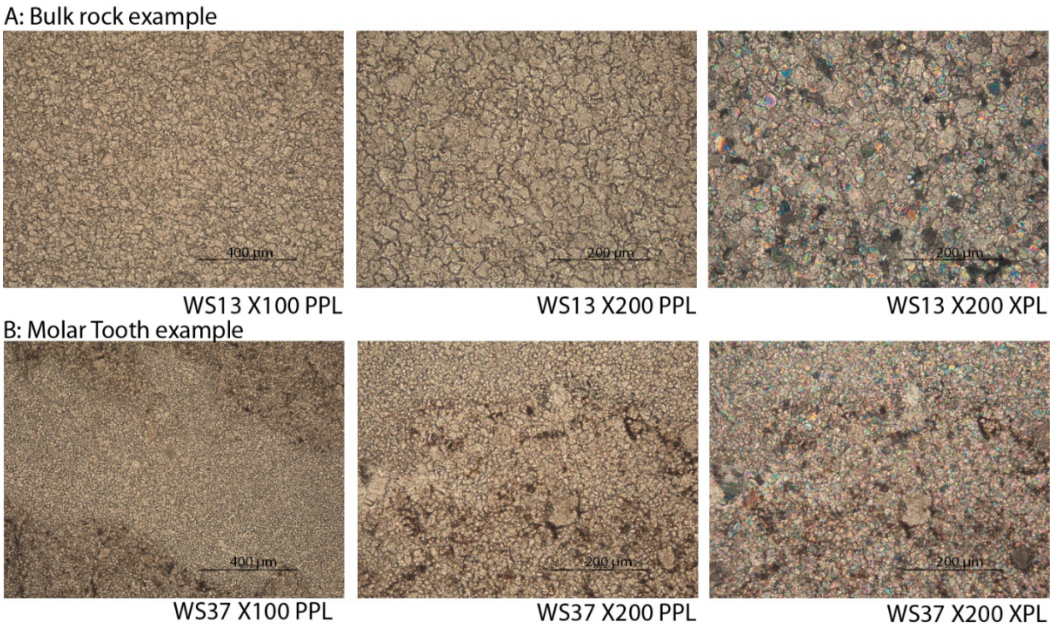

Figure S4: Micrographic images of two samples at different magnifications. A: WS13, bulk rock example of the Wangshan Fm; B: WS37, Calcite microspar cements (used to be named as Molar Tooth structure) example of the Wangshan Fm. PPL: plane-polarized light; XPL: crossed-polarized light.

Some authors put particular emphasis on Mn, Sr, Mg and Ca to understand the degree of alteration associated with meteoric diagenesis and dolomitization (Denison et al., 1994; Korte et al., 2005; van Geldern et al., 2006; Mii et al., 1997). Due to their contrasting distribution coefficients in calcite, the Mn/Sr ratios has been most widely used (Denison et al., 1994; Montanez et al., 1996), whereby samples with the lowest Mn/Sr ratios are deemed likely to have undergone less post-depositional alteration. Figure S5 shows various proposed Mn and Sr cut-offs plotted alongside the Sr and Mn contents of the Huaibei samples.

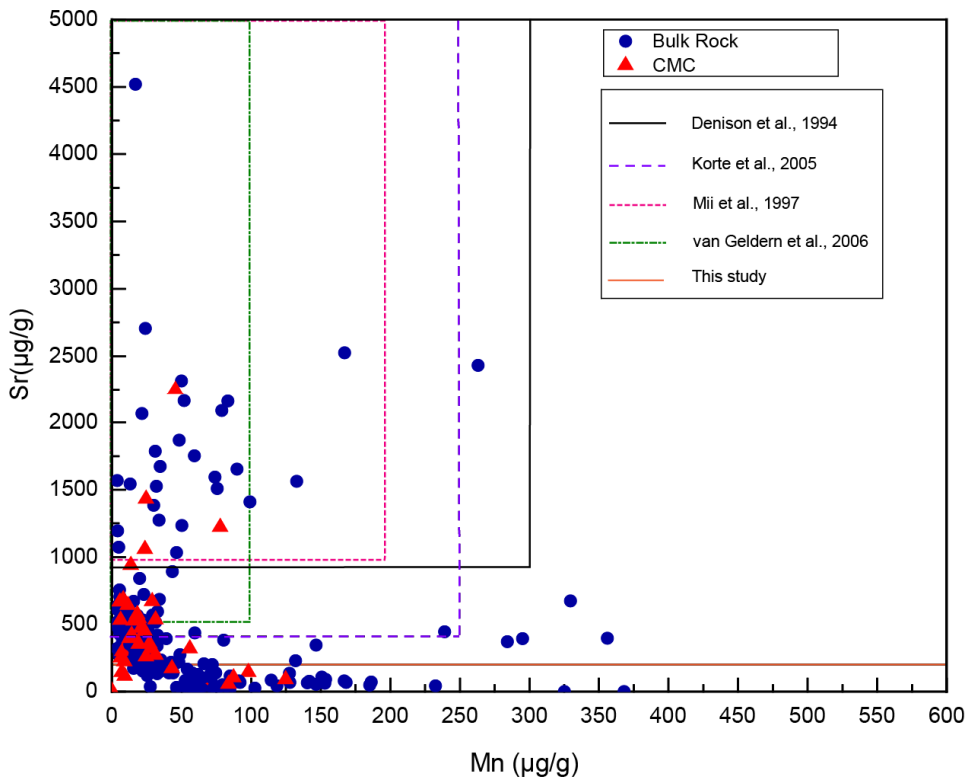

Figure S5: Sr and Mn content of Huaibei samples and trace element static thresholds from some previous publications (Denison et al., 1994; Korte et al., 2005; van Geldern et al., 2006; Mii et al., 1997). A Sr content line of 200 (μg/g) was added, as one of the principles of sample screening of this study.

In our study, a combination of petrological screening, assessment based on a low Mg/Ca ratio, high Sr content, low Mn/Sr ratio (Fig. S6) and low Rb content was carried out (Fig. S7).

In total, from 235 bulk samples and 37 samples containing CMC, 59 bulk samples and 30 CMC samples passed the screening and so were regarded to hold promise to retain an original seawater signal, especially for their Sr isotope values. All 89 Sr isotopic values have been used to fill the c. 980 Ma – c. 920 Ma gap in the existing Neoproterozoic seawater $^{87}Sr/^{86}Sr$ curve.

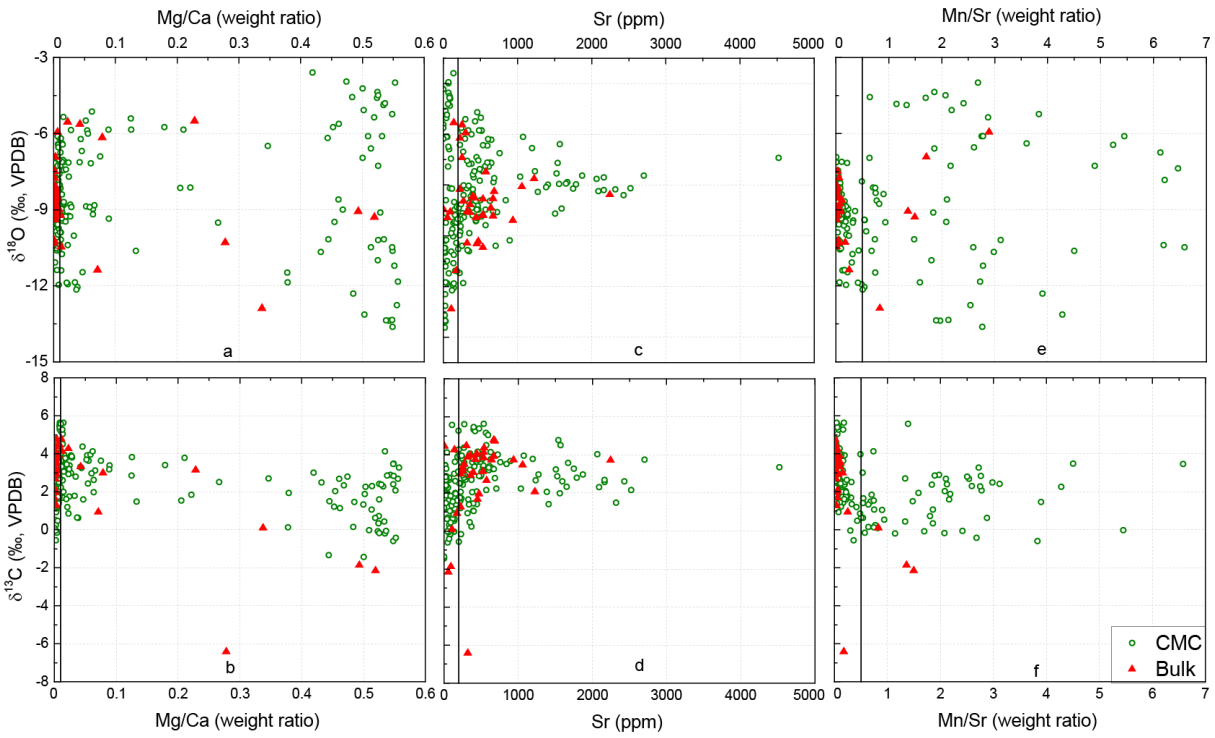

Figure S6: Cross plots of Carbon isotopes and elemental composition. Three lines are added to the plots to indicate the quality of the samples. Mg/Ca = 0.025 (weight ratio), used as the cut-off of low-Mg calcite (Veizer, 1983); Sr content of 200 (µg/g) and Mn/Sr weight ratio of 0.5 (Denison et al., 1994; Montanez et al., 1996).

Rb correction: following ICP-MS measurement of Rb/Sr ratios of the same second leach, most chosen samples for Sr isotope analysis could be corrected for radioactive decay of ^{87}Rb since deposition (Table S1, Fig. S7). Some corrections are missing due to the samples' low Rb concentrations or other unsuccessful analysis. Most Rb corrections resulted in insignificant changes to the measured isotopic ratios. 24 out of 101 samples analysed for Sr isotopes required Rb corrections greater than $1x10^{-4}$, but most of these samples did not pass the initial screening. Due to the inherent uncertainties associated with Rb-decay correction, ^{87}Sr/^{86}Sr values used to

constrain seawater composition and the secular curve were not the Rb corrected values, but the measured ones.

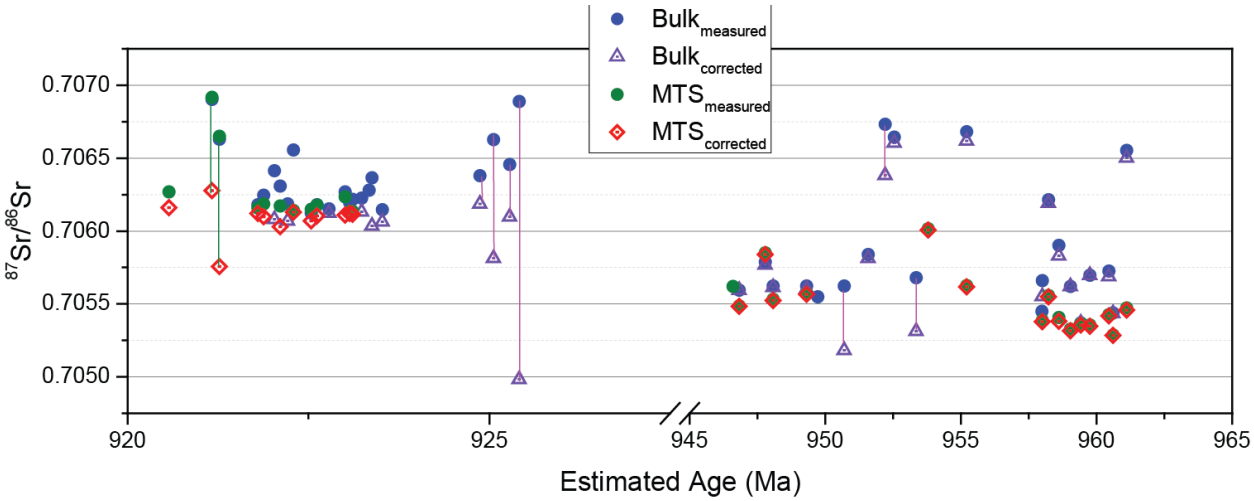

Figure S7: The measured and Rb-corrected $^{87}Sr/^{86}Sr$ values for samples of the Huaibei group.

Updated compilation of Neoproterozoic seawater $^{87}/^{86}Sr$

Significant progress has been made towards a Neoproterozoic seawater $^{87}Sr/^{86}Sr$ curve (Derry et al., 1992; Shields, 1999; Halverson et al., 2007; Kuznetsov et al., 2017). The most widely used curve to date (Halverson et al., 2007, 2010, 2009) compiles apparently least-altered bulk rock data, selected on the basis of their Sr concentrations and elemental compositions. Most recently, Cox et al. (2016) have added further data to the compilation, which includes data from Kaufman et al. (1993), Burns et al. (1994), Knoll et al. (1995), Misi and Veizer (1998), Calver (2000), Yoshioka et al. (2003) and Pokrovskii et al. (2006), with additional published data from Bartley et al. (2001), Kuznetsov et al. (2006), Melezhik et al. (2009), Rooney et al. (2014) and Bold et al. (2016), extending the compilation to 1050 Ma. In these studies, samples with inadequate age control were assigned ages by calibrating carbon isotope data against inferred trends in global ocean $\delta^{13}C_{carb}$ and basic thermal subsidence modelling (Halverson et al., 2002) and by assuming constant sediment accumulation rates.

All attempts to reconstruct a Neoproterozoic Sr isotope curve document a significant rise in seawater $^{87}Sr/^{86}Sr$ ratio over the course of the Neoproterozoic, from about 0.705 to 0.709, which remains speculative in its detail. This, together with the non-uniqueness of most, if not all carbon isotope trends, leaves considerable room for ambiguity (Melezhik et al., 2015). As a result, existing data are sparsely distributed, whilst any extended successions with substantial amounts of data but poor age control, such as those in Siberia and the Urals (e.g. Kuznetsov et al., 2006, 2017), are difficult to correlate with data from other regions of the world (cf. Cox et al., 2016). Nevertheless, the demonstrated existence of primary trends in seawater $^{87}Sr/^{86}Sr$ highlights the potential of SIS for both stratigraphic correlation and environmental interpretation of Neoproterozoic events, provided that suitably well-preserved samples of marine authigenic minerals (generally carbonates) can be identified and can be placed within the improving, global stratigraphic framework.

This study improves Neoproterozoic SIS by specifically targeting demonstrably well-preserved and age-constrained examples of early diagenetic calcite microspar cements (CMC, previously referred to as molar tooth structure due to the outward appearance of some cavities) on the North China craton to fill an acknowledged gap in the record between c.980 to c.920 Ma (Kuznetsov et al., 2017) towards a new Sr isotope curve for Neoproterozoic seawater (Fig. 2).

Discussion and test of the age model

Using the preliminary $^{87}Sr/^{86}Sr$ curve defined by the Huaibei data, we can return to the question of the reliability of the age model. The magnitudes of $^{87}Sr/^{86}Sr$ changes were found to be approximately 0.0006 from the Jiayuan to the Jiudingshan Fm, followed by a rise of ~0.0004 before a slight dip of ~0.0001 and then another ~0.0006 increase during the final rise through the

Wangshan Fm. If these absolute values are taken as conservative estimates of the total change, this would indicate that seawater $^{87}Sr/^{86}Sr$ changed by at least ~0.0017.

Fig. S8 shows the rate of change of Sr isotope composition of the global ocean through the Phanerozoic, based on a LOWESS Fit to reported data (McArthur et al., 2012). The mean of the rate of change based on this LOWESS fit is 0.000026 per million years if all the rates of change are treated as absolute values, by neglecting whether $^{87}Sr/^{86}Sr$ is rising or falling. Over short intervals, the rate of change can vary widely, and is seldom zero, but at longer timescales of >20-30 million years the data consistently approach the long-term mean. If we assume 0.000026 per m.y. to be a representative rate of change of seawater $^{87}Sr/^{86}Sr$ for Tonian time, then the postulated shift of 0.0017 for the studied Neoproterozoic strata would represent ~65 Ma, which is consistent with the preliminary age model, i.e. 980 to 920 Ma.

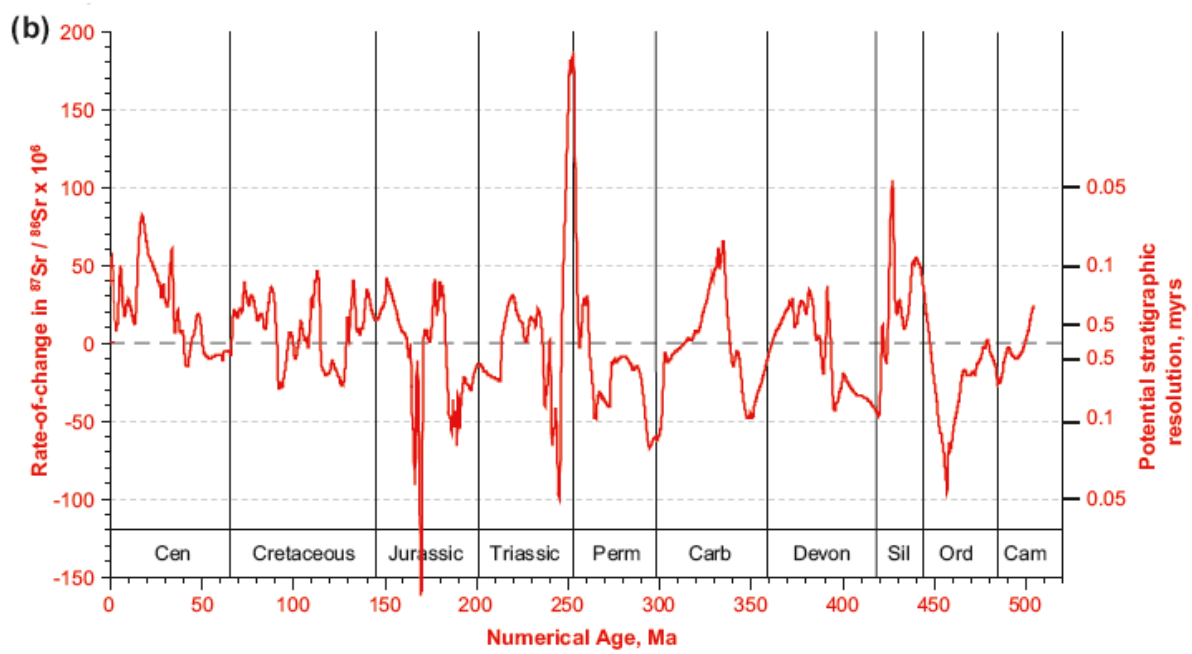

Fig. S8 Rate of change with time of $^{87}Sr/^{86}Sr$ through the Phanerozoic, showing temporal differences in the potential stratigraphic resolution of strontium isotope stratigraphy from McArthur et al. (2012).

As the rate of change of seawater $^{87}Sr/^{86}Sr$ varies over time, as shown in Fig. S5, we must add the caveat here that our duration estimate carries with it an error bar of uncertain magnitude. Clearly, the rate of change of seawater $^{87}Sr/^{86}Sr$ will depend on fluxes and reservoirs of ocean Sr that are currently unconstrained. For argument's sake, were we to take the maximum rate of change during the Phanerozoic, i.e. 0.000192, then the time taken to deposit the studied strata could have been as short as 8.33 Ma. However, this seems most unlikely because this anomalously extreme rate of change occurred during one unidirectional change, while the Huaibei curve changes direction multiple times, during which the rate of change fell to zero. Obviously, the mean rate of change used here is from the Phanerozoic; it is only used here to test the viability of the suggested age model of 980 to 920 Ma.

TABLE 1. Rb correction result for Sr isotope values of the Huaibei Group

Sample	Estimated age (Ma)	BULK				CMC			
		$^{87}Sr/^{86}Sr$	Rb/Sr	Rb-Corr	$^{87}Sr/^{86}S_{corr}$	$^{87}Sr/^{86}S$	Rb/Sr	Rb-Corr	$^{87}Sr/^{86}Sr_{corr}$
JSZ2	920.00	0.706521				0.706135			
JSZ4	920.02	0.706123				0.706089			
JSZ5	920.14	0.706109	4.78E-03	1.77E-04	0.705932				
WS48	920.57					0.706268	2.89E-03	1.07E-04	0.706161
WS46	921.17	0.706904				0.706918	1.73E-02	6.40E-04	0.706278
WS45	921.27	0.70663				0.706651	2.41E-02	8.94E-04	0.705757
WS44	921.37						1.14E-02	4.23E-04	
WS39	921.80	0.706181				0.706158	1.02E-03	3.78E-05	0.706121
WS38	921.88	0.706246				0.706187	2.41E-03	8.97E-05	0.706097
WS37	922.03	0.706415	8.97E-03	3.33E-04	0.706082				
WS36	922.11	0.706309				0.706173	3.89E-03	1.44E-04	0.706029
WS35	922.21	0.706187	3.19E-03	1.19E-04	0.706068				
WS34	922.29	0.706555				0.70614	2.80E-04	1.03E-05	0.70613
WS33	922.54	0.706123				0.70615	2.16E-03	8.03E-05	0.70607
WS32	922.62	0.70618				0.706178	2.06E-03	7.65E-05	0.706104
WS30	922.78	0.706152	7.60E-04	2.84E-05	0.706124				
WS26	923.01	0.706268				0.706234	3.32E-03	1.23E-04	0.706111
WS25	923.07	0.706195				0.706135	3.80E-04	1.42E-05	0.706121
WS24	923.11	0.706217				0.706134	5.40E-04	2.01E-05	0.706114
WS21	923.23	0.706227	2.56E-03	9.53E-05	0.706132				
WS19	923.34	0.706281							
WS18	923.38	0.706365	8.84E-03	3.29E-04	0.706036				
WS15	923.52	0.706146	2.24E-03	8.33E-05	0.706063				
WS11	924.87	0.70638	5.22E-03	1.94E-04	0.706186				
WS09	925.06	0.706627	2.18E-02	8.12E-04	0.705815				
WS04	925.28	0.706456	9.60E-03	3.58E-04	0.706098				
WS01	925.41	0.706888	5.11E-02	1.90E-03	0.704983				
YJZ9	940.39					0.706306	9.69E-04	3.67E-05	0.706269
YJZ3	943.30	0.707073	1.32E-03	5.00E-05	0.707023				
LS158	946.61					0.705621			
LS156	946.84	0.705596	6.00E-05	2.41E-06	0.705594	0.705488	1.10E-04	4.29E-06	0.705484
LS151	947.79	0.705787	5.20E-04	1.98E-05	0.705767	0.705851	2.80E-04	1.09E-05	0.70584
LS147	948.08	0.705624	2.70E-04	1.03E-05	0.705614	0.705531	1.70E-04	6.65E-06	0.705524
LS140	949.32	0.705622	4.90E-04	1.88E-05	0.705603	0.705569	7.00E-05	2.63E-06	0.705566
LS137	949.73	0.70555							
LS133	950.70	0.705623	1.15E-02	4.40E-04	0.705183				
LS128	951.59	0.70584	7.10E-04	2.73E-05	0.705813				
LS122	952.21	0.706732	9.09E-03	3.49E-04	0.706383				

LS117	952.54	0.706644	1.02E-03	3.92E-05	0.706605				
LS108	953.35	0.70568	9.52E-03	3.66E-04	0.705314				
LS103	953.80					0.706015	2.30E-04	8.90E-06	0.706006
LS87	955.21	0.706681	1.59E-03	6.12E-05	0.70662	0.705625	2.20E-04	8.49E-06	0.705617
LS46	957.99	0.705449							
LS45	958.01	0.70566	2.80E-03	1.08E-04	0.705552	0.705387	2.50E-04	9.65E-06	0.705377
LS40B	958.24	0.706215	6.00E-04	2.33E-05	0.706192	0.705558	2.60E-04	9.86E-06	0.705548
LS34	958.62	0.705902	1.87E-03	7.22E-05	0.70583	0.705406	6.10E-04	2.34E-05	0.705383
LS29	959.03	0.705621			0.705621	0.705326	2.60E-04	1.02E-05	0.705316
LS26	959.43	0.70537			0.70537	0.705364	2.00E-04	7.82E-06	0.705356
LS24	959.76	0.705698			0.705698	0.705355	1.60E-04	6.36E-06	0.705349
LS20	960.46	0.705726	9.80E-04	3.80E-05	0.705688	0.705426	1.80E-04	7.06E-06	0.705419
LS19	960.60	0.705439	1.00E-04	3.92E-06	0.705435	0.705287	9.00E-05	3.49E-06	0.705284
LS13	961.12	0.706554	1.37E-03	5.32E-05	0.706501	0.705471	3.40E-04	1.32E-05	0.705458
ZW-H2	973.72	0.706088				0.705635			
ZW-H1	973.82		9.77E-05			0.706056	7.23E-03	2.84E-04	0.705772
ZW-M	974.02	0.706077				0.705969	8.69E-03	3.41E-04	0.705628
ZW-L	974.13	0.705768	2.90E-03	1.10E-04	0.705654	0.70586			
ZW-U	974.23	0.705711				0.705734	2.23E-03	8.77E-05	0.705646
JY1	975.05	0.705775							
JY2	975.07	0.705823							
JY3	975.09	0.708505							
JY4	976.52	0.705786	1.81E-03	7.14E-05	0.705715				
JY5	978.16	0.705851							
JY6	978.57	0.706414	9.86E-03	3.89E-04	0.706025				
JY7	979.59	0.706737	1.05E-02	4.14E-04	0.706323				
JY8	980.00	0.708008	2.28E-02	9.02E-04	0.707106				

TABLE 2. C isotope values and elemental ratios of the carbonate samples from the Huaibei Group

Strat. Height (m)	Estimate Age (Ma)	Sample	Bulk- $\delta^{13}C_{PDB}$ (‰)	CMC $\delta^{13}C_{PDB}$ (‰)	Bulk Mg/Ca	CMC Mg/Ca	Bulk Mn/Sr	CMC Mn/Sr	Bulk Sr (μg/g)	CMC Sr (μg/g)
2924.2	920	JSZ2	3.72	4.08						
2910.2	920.31	JSZ4	4.47	4.35						
2904.2	920.43	JSZ5	3.96	4.66						
2903.2	920.45	WS48	2.7		0.347	0.057	1.335	0.683	68.8	143.3
2884.2	920.84	WS47	2.8		0.474		2.505		67.1	
2874.2	921.05	WS46	3.01	3.15	0.419	0.228	0.529		134.0	169.2
2869.2	921.15	WS45	2.44		0.054	0.088	0.119	1.026	253.8	69.2
2864.2	921.25	WS44	2.06		0.007		0.065		224.2	
2860.2	921.33	WS43	2.71		0.009		0.074		293.5	
2857.2	921.39	WS42	3.26		0.008		0.02		590.7	
2852.2	921.5	WS41	3.36		0.016		0.023		523.4	
2847.2	921.6	WS40	3.39		0.024		0.017		409.1	
2843.2	921.68	WS39	3.63	4.27	0.055	0.023	0.02	0.049	377.5	143.0
2839.2	921.76	WS38	4.39		0.046	0.034	0.019	0.077	264.9	115.6
2832.2	921.91	WS37	4.13		0.062		0.013		459.1	
2828.2	921.99	WS36	3.42	3.32	0.179	0.042	0.057	0.095	241.5	251.2
2823.2	922.09	WS35	3.88		0.028		0.008		512.8	
2819.2	922.17	WS34	3.79	4.47	0.21	0.007	0.028	0.024	514.8	300.6
2807.2	922.42	WS33	3.83		0.126	0.051	0.025	0.069	482.4	365.6
2803.2	922.5	WS32	3.7		0.052	0.033	0.013	0.051	425.8	360.0
2798.2	922.6	WS31	3.77		0.018		0.006		628.1	
2795.2	922.67	WS30	3.13		0.016		0.006		507.6	
2792.2	922.73	WS29	3.26		0.044		0.007		645.1	
2790.2	922.77	WS28	3.21		0.024		0.014		603.9	
2786.2	922.85	WS27	3.18		0.089		0.026		336.9	
2784.2	922.89	WS26	2.86	2.99	0.125	0.079	0.03	0.153	294.1	223.3
2781.2	922.95	WS25	3.45	3.15	0.02	0.003	0.009	0.025	527.3	253.1
2779.2	922.99	WS24	2.97		0.06	0.003	0.019	0.033	343.8	417.0
2777.2	923.04	WS23	2.87		0.008		0.006		490.4	
2775.2	923.08	WS22	3.96		0.007		0.004		1072.3	
2773.2	923.12	WS21	3.31		0.042		0.009		645.7	
2771.2	923.16	WS20	3.07		0.015		0.011		319.4	
2768.2	923.22	WS19	3.41		0.007		0.006		610.0	

2766.2	923.26	WS18	3.64		0.075		0.012		445.9	
2763.2	923.32	WS17	3.63		0.011		0.007		756.0	
2761.2	923.36	WS16	3.79		0.008		0.003		1194.0	
2759.2	923.4	WS15	4.51		0.014		0.002		1567.5	
2749.2	923.61	WS14	3.64		0.008		0.008		493.1	
2747.2	923.65	WS13	3.33		0.012		0.008		600.5	
2743.2	923.73	WS12	2.24		0.011		0.008		705.7	
2693.2	924.76	WS11	5.17		0.011		0.03		565.0	
2688.2	924.86	WS10	4.01		0.01		0.095		341.0	
2684.2	924.94	WS09	5.04		0.013		0.055		593.2	
2681.7	924.99	WS08	5.34		0.009		0.065		396.1	
2679.7	925.04	WS07	5.27		0.009		0.077		418.7	
2677.7	925.08	WS06	5.47		0.008		0.074		398.9	
2675.2	925.13	WS05	5.64		0.015		0.041		532.6	
2673.2	925.17	WS04	5.39		0.009		0.055		470.3	
2670.7	925.22	WS03	5.63		0.009		0.178		274.3	
2668.7	925.26	WS02	5.29		0.013		0.163		194.7	
2666.7	925.3	WS01	5.59		0.01		1.389		108.5	
1916.7	940.69	YJZ9	3.37							
1907.7	940.87	YJZ8	3.61							
1870.7	941.63	YJZ7	2.1							
1852.7	942	YJZ6	2.03							
1836.7	942.33	YJZ5	2.6							
1792.7	943.23	YJZ4	4.13							
1775.7	943.58	YJZ3	2.16							
1731.7	944.48	YJZ2	1.92							
1701.7	945.1	YJZ1	1.15							
1641.7	946.33	LS160	2.31		0.514		2.594		22.8	
1625.7	946.65	LS159	1.5		0.445		1.477		31.5	
1615.7	946.86	LS158	2.8		0.034		0.066		269.6	
1609.7	946.98	LS157	3.68		0.011		0.049		892.2	
1604.7	947.09	LS156	2.09	3.74	0.005	0.002	0.137	0.015	435.9	939.9
1594.7	947.29	LS155	2.81		0.005		0.018		1785.7	
1588.7	947.41	LS154	3.58		0.003		0.021		1672.9	
1576.7	947.66	LS153	4.04		0.005		0.01		2065.2	
1566.7	947.86	LS152	2.88		0.004		0.021		1524.8	
1558.7	948.03	LS151	1.41	2.07	0.004	0.002	0.07	0.064	1410.2	1222.2
1556.7	948.07	LS150	3.28		0.003		0.034		1751.3	
1554.7	948.11	LS149	2.98		0.002		0.027		1273.3	

1552.7	948.15	LS148	2.33		0.003		0.054		1653.5	
1544.7	948.32	LS147	2.62	3.47	0.004	0.002	0.047	0.023	1592.6	1058.0
1534.7	948.52	LS146	3.24		0.003		0.05		1507.3	
1525.7	948.71	LS145	2.68		0.003		0.041		1233.1	
1515.7	948.91	LS144	2.57		0.002		0.024		2163.0	
1509.7	949.03	LS143	2.97		0.003		0.026		1868.5	
1497.7	949.28	LS142	2.06	2.81	0.003		0.022		1383.1	
1489.7	949.44	LS141	1.98		0.002	0.001	0.085	0.017	1561.0	1432.1
1484.7	949.55	LS140	2.31	3.72		0.002	0.038	0.02	2087.7	2246.3
1480.7	949.63	LS139	3.99		0.001		0.49		673.2	
1470.7	949.83	LS138	2.61		0.013		0.108		2431.5	
1464.7	949.96	LS137	1.49		0.002		0.022		2316.0	
1459.7	950.06	LS136	3.35		0.007		0.004		4518.8	
1447.7	950.31	LS135	2.16		0.003		0.066		2522.7	
1427.7	950.72	LS134	2.69		0.003		0.039		2160.2	
1417.7	950.92	LS133	2.24		0.002		0.045		1032.7	
1407.7	951.13	LS132	3.75		0.003		0.009		2704.0	
1397.7	951.33	LS131	5.27		0.003		0.004		--	
1387.7	951.54	LS130	4.78		0.002		0.009		1540.9	
1380.7	951.68	LS129	2.79		0.002		0.05		685.5	
1374.7	951.8	LS128	2.55		0.004		0.108		--	
1366.7	951.97	LS127	2.04		0.001		0.211		381.0	
1361.7	952.07	LS126	1.08		0.002		0.748		394.6	
1357.7	952.15	LS125	1.05		0.004		0.898		396.8	
1352.7	952.25	LS124	0.24		0.002		0.767		370.6	
1348.7	952.34	LS123	0.1				0.815		--	
1344.7	952.42	LS122	1.66		0.003		0.546		--	
1340.7	952.5	LS121	1.41		0.003		0.539		444.3	
1340.5	952.5	LS120	0.54				0.936		136.4	
1338.5	952.55	LS119	-0.16		0.004		0.573		230.4	
1331.5	952.69	LS118	-0.56		0.002		0.361		200.0	
1328.5	952.75	LS117	0.48		0.005		0.427		344.0	
1323.5	952.85	LS116	0.63		0.039		0.538		138.9	
1318.5	952.96	LS115	0.65		0.037		0.501		119.0	
1314.5	953.04	LS114	0.86		0.023		0.484		128.0	
1309.5	953.14	LS113	1.35		0.005		0.324		166.9	
1306.5	953.2	LS112	1.49		0.133		0.677		105.8	
1302.5	953.28	LS111	1.19		0.021		0.417		138.7	
1299.5	953.35	LS110	2.07		0.552		2.775		30.4	

1294.5	953.45	LS109	-0.03		0.003		0.298		137.3	
1289.5	953.55	LS108	2.38		0.008		0.189		--	
1285.5	953.63	LS107	2.05		0.454		2.081		35.5	
1279.5	953.76	LS106	2.69		0.461		2.101		36.1	
1275.5	953.84	LS105	1.95		0.379		1.585		50.1	
1271.5	953.92	LS104	2.26		0.503		4.28		18.7	
1267.5	954	LS103	2.42	-6.42	0.525	0.278	3.113	0.175	23.5	320.6
1262.5	954.1	LS102	2.5		0.432		2.98		24.6	
1258.5	954.19	LS101	3.48		0.549		4.501		14.5	
1254.5	954.27	LS100	3.46		0.548	0.337	6.581	0.828	12.9	105.7
1249.5	954.37	LS99	0.72		0.525		1.803		47.5	
1244.5	954.47	LS98	0.34		0.524		1.86		68.8	
1241.5	954.54	LS97	-0.2		0.535		1.141		80.1	
1236.5	954.64	LS96	-0.07		0.523		1.693		90.7	
1231.5	954.74	LS95	-0.16		0.525		2.072		80.5	
1226.5	954.84	LS94	0.16		0.483		0.637		82.6	
1222.5	954.92	LS93	1.34		0.5		0.636		102.3	
1218.5	955.01	LS92	0.44		0.534		1.332		86.0	
1215.5	955.07	LS91	-0.06		0.536		2.413		63.5	
1212.5	955.13	LS90	0.64		0.519		2.875		41.2	
1208.5	955.21	LS89	2.29		0.532		2.75		53.4	
1202.5	955.34	LS88	2.52		0.007	0	0.195	0.052	218.8	450.0
1199.5	955.4	LS87	1.66	1.95	0.009	0.001	0.076	0.045	324.3	473.7
1195.5	955.48	LS86	0.14		0.378		0.744		74.1	
1192.5	955.54	LS85	2.41		0.1		0.288			
1182.5	955.75	LS84	1.88		0.502		2.186		28.8	
1178.5	955.83	LS83	2.33		0.468					
1175.5	955.89	LS82	1.15		0.462					
1168.5	956.03	LS81	-0.01		0.509		5.446		42.7	
1158.5	956.24	LS80	1.23		0.452					
1156.5	956.28	LS79	0.67		0.362					
1146.5	956.48	LS78	-0.21		0.373		17.503			
1142.5	956.57	LS77	-1.44		0.5					
1140.5	956.61	LS76	-1.33		0.444					
1138.5	956.65	LS75	-0.59		0.548		3.833		48.4	
1137.5	956.67	LS74	-0.42		0.552		2.681		69.5	
1136.5	956.69	LS73	1.06		0.513		1.858		76.4	
1134.5	956.73	LS72	1.61		0.525		2.166		64.9	
1132.5	956.77	LS71	2.38		0.529		1.839		33.7	

1130.5	956.81	LS70	1.59	0.93	0.047	0.071	0.217	0.25	221.1	172.8
1128.5	956.85	LS69	2.52	-1.87	0.266	0.493	0.321	1.362	206.1	91.6
1125.5	956.91	LS68	2.89		0.544		1.97		27.1	
1122.5	956.98	LS67	2.85	-2.16	0.538	0.519	1.892	1.493	30.5	56.3
1119.5	957.04	LS66	2.41		0.548		2.124		23.6	
1117.5	957.08	LS65	2.69		0.556		2.539		25.1	
1113.5	957.16	LS64	3.28		0.557		2.723		28.0	
1109.5	957.24	LS63	1.47		0.485		3.9		26.4	
1108.5	957.26	LS62	2.84		0.548		2.762		20.2	
1107.5	957.28	LS61	1.7		0.012		0.123		182.3	
1105.5	957.32	LS60	1.42		0.005		0.167		160.3	
1102.5	957.39	LS59	1.69		0.013		0.315		139.8	
1097.5	957.49	LS58	1.72		0.008		0.212		120.2	
1091.5	957.61	LS57	1.79		0.033		0.247		132.0	
1087.5	957.69	LS56	2.01		0.014		0.145		151.5	
1083.5	957.78	LS55	1.73		0.006		0.151		233.9	
1082	957.81	LS54	1.21		0.006		0.122		220.1	
1080	957.85	LS53	1.75		0.024		0.218		212.2	
1077	957.91	LS52	1.61		0.019		0.183		176.4	
1076.9	957.91	LS51	1.97		0.064		0.215		157.5	
1075	957.95	LS50	2.63		0.063		0.231		149.5	
1073	957.99	LS49	3.34		0.014		0.119		256.8	
1070	958.05	LS48	3.13		0.066		0.158		188.1	
1068	958.09	LS47	3.75		0.016		0.049		461.4	
1065	958.16	LS46	4.03		0.007		0.032		722.8	
1064	958.18	LS45	3.92	3.9	0.053	0.006	0.191	0.088	181.8	318.8
1062	958.22	LS44	3.78	4.05	0.017	0.003	0.093	--	254.6	443.9
1060	958.26	LS43	3.96	4.37	0.059	0.002	0.13	--	210.0	539.4
1058	958.3	LS42	4.51		0.013	0.027	0.033	0.094	566.7	259.6
1055	958.36	LS41	3.93		0.027		0.054		405.2	
1053	958.4	LS40	3.97	3.76	0.016	0.004	0.094	0.034	236.3	421.5
1051	958.44	LS39	2.95		0.006	0.011	0.048	0.036	500.2	543.7
1048	958.5	LS 38	3.64	3.26						
1044	958.59	LS37	2.15	2.92	0.006	0.003	0.051	0.076	569.9	357.7
1041.5	958.64	LS36	3.6		0.006		0.061		274.1	
1037.5	958.72	LS35	3.52	3.08	0.008	0.006	0.024	0.032	840.1	395.2
1034.5	958.78	LS34	3.64	3.51	0.009	0.003	0.165	0.116	145.4	271.6
1030.5	958.86	LS33	3.81		0.028		0.067		385.0	
1025.5	958.97	LS32	3.32	3.97	0.012	0.002	0.068	0.055	248.6	354.8

1021.5	959.05	LS31	3.9		0.008		0.041		449.7	
1019.5	959.09	LS30	3.26		0.005		0.023		670.4	
1014.5	959.19	LS29	2.9	3.73	0.004	0.003	0.04	0.018	471.7	642.5
1008.5	959.31	LS28	2.69	3.85	0.005	0.003	0.059	0.059	369.4	534.0
1001.5	959.46	LS27	4.16		0.007		0.019		625.9	
995.5	959.58	LS26	4.17	4.47	0.006	0.009	0.033	0.02	450.8	4.9
989.5	959.7	LS25	2.99	4.12	0.027		0.063		278.3	
979.5	959.91	LS24	3.22	3.93	0.016	0.007	0.048	0.043	352.2	671.6
972.5	960.05	LS23	1.46	3.12	0.007	0.002	0.1	0.03	392.3	525.1
963.5	960.24	LS22	2.93	4.13	0.023	0.012	0.064	0.012	252.6	532.6
953.5	960.44	LS21	4.13		0.535		0.735		37.5	
945.5	960.61	LS20	4.09	4.38	0.012		0.037		350.1	
938.5	960.75	LS19	3.38	4.78	0.089	0.011	0.101	0.008	231.2	668.9
934.5	960.83	LS18	3.8		0.019		0.029		462.9	
931.5	960.89	LS17	3.8	4.74	0.008	0.004	0.061	0.012	514.3	684.8
927.5	960.98	LS16	4.25		0.007		0.09		172.9	
923.5	961.06	LS15	4.29		0.005		0.097		197.1	
918.5	961.16	LS14	1.4	3.03	0.007		0.047		336.7	
913.5	961.26	LS13	0.94	2.66	0.003	0.002	0.076	0.032	317.5	574.5
909.5	961.34	LS12	3.16	1.26	0.011	0.004	0.082	0.04	233.5	224.4
906.5	961.41	LS11	1.85		0.221		0.703		85.8	
902.5	961.49	LS10	1.54	2.12	0.205		0.74		115.0	
897.5	961.59	LS9	1.92							
894.5	961.65	LS8	1.88							
892.5	961.69	LS7	2.25							
889.5	961.76	LS6	2.06							
887.5	961.8	LS5	2							
885.5	961.84	LS4	1.61							
877.5	962	LS3	1.89							
874.5	962.06	LS2	1.98							
873	962.09	LS1	1.89	1.99						
873	962.09	NY								
473	970.3	ZW								
307	973.7	ZW-H2	2.83	3.55						
302	973.81	ZW-H1	2.7	2.67						
292	974.01	ZW-M	0.79	2.23						
287	974.11	ZW-L	3.32	2.54						
282	974.22	ZW-U	3.98	3.54						
242	975.04	JY1	2.82							

241	975.06	JY2	2.4							
240	975.08	JY3	3.7							
170	976.51	JY4	3.46							
90	978.15	JY5	2.14							
70	978.56	JY6	2.34							
20	979.59	JY7	2.42							
0	980	JY8	2.12							

REFERENCES:

Bartley, J.K., Semikhatov, M.A., Kaufman, A.J., Knoll, A.H., Pope, M.C., and Jacobsen, S.B., 2001, Global events across the Mesoproterozoic-Neoproterozoic boundary: C and Sr isotopic evidence from Siberia: Precambrian Research, v. 111, p. 165–202, doi: 10.1016/S0301-9268(01)00160-7.

Bishop, J.W., Sumner, D.Y., and Huerta, N.J., 2006, Molar tooth structures of the Neoarchean Monteville formation, Transvaal Supergroup, South Africa. I: Constraints on microcrystalline CaCO3 precipitation: Sedimentology, v. 53, p. 1049–1068, doi: 10.1111/j.1365-3091.2006.00801.x.

Bold, U., Smith, E.F., Rooney, A.D., Bowring, S.A., Buchwaldt, R., Dudás, F.Ö., Ramezani, J., Crowley, J.L., Schrag, D.P., and Macdonald, F.A., 2016, Neoproterozoic stratigraphy of the zavkhan terrane of Mongolia: The backbone for cryogenian and early ediacaran chemostratigraphic records: American Journal of Science, v. 315, p. 1–63, doi: 10.2475/01.2016.01.

Burns, S.J., Haudenschild, U., Matter, A., Institut, G., Bern, U., Baltzerstrasse, I., and Bern, C.-, 1994, The strontium isotopic composition of carbonates from the late Precambrian (~ 560-540 Ma) Huqf Group of Oman: v. 111.

Calver, C.R., 2000, Isotope stratigraphy of the Ediacarian (Neoproterozoic III) of the Adelaide Rift Complex , Australia , and the overprint of water column stratification: v. 100, p. 121–150.

Chaves, A.D.O., Ernst, R.E., Söderlund, U., Wang, X., and Naeraa, T., 2018, The 920 – 900 Ma Bahia-Gangila LIP of the São Francisco and Congo cratons and link with Dashigou-Chulan LIP of North China craton : New insights from U-Pb geochronology and geochemistry: Precambrian Research, p. 0–1, doi: 10.1016/j.precamres.2018.08.023.

Cox, G.M., Halverson, G.P., Stevenson, R.K., Vokaty, M., Poirier, A., Kunzmann, M., Li, Z.-X., Denyszyn, S.W., Strauss, J. V., and Macdonald, F.A., 2016, Continental flood basalt weathering as a trigger for Neoproterozoic Snowball Earth: Earth and Planetary Science Letters, v. 446, p. 89–99, doi: 10.1016/j.epsl.2016.04.016.

Denison, R.E., Koepnick, R.B., Fletcher, A., Howelf, M.W., and Callaway, W.S., 1994, Criteria for the retention of original seawater $^{87}Sr/^{86}Sr$ in ancient shelf limestones: Chemical Geology: Isotope Geoscience Section, v. 112, p. 131–143.

Derry, L.A., Kaufman, A.J., and Jacobsen, S.B., 1992, Sedimentary cycling and environmental change in the late Proterozoic: evidence from stable isotopes: Geochimica et Cosmochimica Acta, v. 56, p. 1317–1329.

Dong, L., Xiao, S., Shen, B., Yuan, X., Yan, X., and Peng, Y., 2008, Restudy of the worm-like carbonaceous compression fossils Protoarenicola, Pararenicola, and Sinosabellidites from early Neoproterozoic successions in North China: Palaeogeography, Palaeoclimatology, Palaeoecology, v. 258, p. 138–161, doi: 10.1016/j.palaeo.2007.05.019.

Ernst, R.E., Wingate, M.T.D., Buchan, K.L., and Li, Z.X., 2008, Global record of 1600-700 Ma Large Igneous Provinces (LIPs): Implications for the reconstruction of the proposed Nuna

(Columbia) and Rodinia supercontinents: Precambrian Research, v. 160, p. 159–178, doi: 10.1016/j.precamres.2007.04.019.

Fairchild, I.J., Herrington, P.M., and Song, T., 2000, Controls on Sr and C isotope compositions of Neoproterozoic Sr-rich limestones of East Greenland and North China: Special Publications of SEPM, v. 67, p. 297–313.

Fu, X., Zhang, S., Li, H., Ding, J., Li, H., Yang, T., Wu, H., Yuan, H., and Lv, J., 2015, New paleomagnetic results from the Huaibei Group and Neoproterozoic mafic sills in the North China Craton and their paleogeographic implications: Precambrian Research, v. 269, p. 90–106, doi: 10.1016/j.precamres.2015.08.013.

Gao, L., Zhang, C., and Chen, S., 2010, Detrital zircon SHRIMP U--Pb age from the Diaoyutai Formation, Xihe Group in Liaodong Peninsula, China and its geological significance: Gelogical BUlletin of China, v. 29, p. 1113–1122.

Gao, L., Zhang, C., Liu, P., Tang, F., Song, B., and Ding, X., 2009, Reclassification of the Meso- and Neoproterozoic chronostratigraphy of North China by SHRIMP zircon ages: Acta Geologica Sinica - English Edition, v. 83, p. 1074–1084.

van Geldern, R., Joachimski, M.M., Day, J., Jansen, U., Alvarez, F., Yolkin, E.A., and Ma, X.P., 2006, Carbon, oxygen and strontium isotope records of Devonian brachiopod shell calcite: Palaeogeography, Palaeoclimatology, Palaeoecology, v. 240, p. 47–67, doi: 10.1016/j.palaeo.2006.03.045.

Halverson, G.P., Dudás, F.Ö., Maloof, A.C., and Bowring, S.A., 2007, Evolution of the $^{87}Sr/^{86}Sr$ composition of Neoproterozoic seawater: Palaeogeography, Palaeoclimatology, Palaeoecology, v. 256, p. 103–129, doi: 10.1016/j.palaeo.2007.02.028.

Halverson, G.P., Hoffman, P.F., Schrag, D.P., and Kaufman, A.J., 2002, A major perturbation of

the carbon cycle before the Ghaub glaciation (Neoproterozoic) in Namibia: Prelude to snowball Earth? Geochemistry Geophysics Geosystems, v. 3, p. 1–24, doi: 10.1029/2001GC000244.

Halverson, G.P., Hurtgen, M.T., Porter, S.M., and Collins, A.S., 2009, Chapter 10 Neoproterozoic-Cambrian Biogeochemical Evolution: Developments in Precambrian Geology, v. 16, p. 351–365, doi: 10.1016/S0166-2635(09)01625-9.

Halverson, G.P., Wade, B.P., Hurtgen, M.T., and Barovich, K.M., 2010, Neoproterozoic chemostratigraphy: Precambrian Research, v. 182, p. 337–350, doi: 10.1016/j.precamres.2010.04.007.

He, T., Zhou, Y., Vermeesch, P., Rittner, M., Miao, L., Carter, A., Pogge von Strandmann, P.A.E., and Shields, G.A., 2016, Measuring the "Great Unconformity" on the North China Craton using new detrital zircon age data: Geological Society, London, Special Publications, v. 448, doi: http://doi.org/10.1144/SP448.14.

Hodgskiss, M.S.W., Kunzmann, M., Poirier, A., and Halverson, G.P., 2018, The role of microbial iron reduction in the formation of Proterozoic molar tooth structures: Earth and Planetary Science Letters, v. 482, p. 1–11, doi: 10.1016/j.epsl.2017.10.037.

Kaufman, A.J., Jacobsen, S.B., and Knoll, A.H., 1993, The Vendian record of Sr and C isotopic variations in seawater: Implications for tectonics and paleoclimate: Earth and Planetary Science Letters, v. 120, p. 409–430, doi: 10.1016/0012-821X(93)90254-7.

Knoll, A.H., Kaufman, A.J., and Semikhatov, M.A., 1995, The carbon-isotopic composition of Proterozoic carbonates: Riphean successions from northwestern Siberia (Anabar Massif, Turukhansk Uplift): American Journal of Science, v. 295, p. 823–850.

Korte, C., Kozur, H.W., and Veizer, J., 2005, δ13C and δ18O values of Triassic brachiopods and

carbonate rocks as proxies for coeval seawater and palaeotemperature: Palaeogeography, Palaeoclimatology, Palaeoecology, v. 226, p. 287–306, doi: 10.1016/j.palaeo.2005.05.018.

Kuang, H., Yongqing, L., Peng, N., and Liu, L., 2011, Geochemistry of the Neoproterozoic molartooth carbonates in Dalian, eastern Liaoning, China, and its geological implications: Earth Science Frontiers (in Chinese), v. 18, p. 25–40.

Kuznetsov, A.B., Bekker, A., Ovchinnikova, G. V., Gorokhov, I.M., and Vasilyeva, I.M., 2017, Unradiogenic strontium and moderate-amplitude carbon isotope variations in early Tonian seawater after the assembly of Rodinia and before the Bitter Springs Excursion: Precambrian Research, v. 298, p. 157–173, doi: 10.1016/j.precamres.2017.06.011.

Kuznetsov, a. B., Semikhatov, M. a., Maslov, a. V., Gorokhov, I.M., Prasolov, E.M., Krupenin, M.T., and Kislova, I. V., 2006, New data on Sr-and C-isotopic chemostratigraphy of the Upper Riphean type section (Southern Urals): Stratigraphy and Geological Correlation, v. 14, p. 602–628, doi: 10.1134/S0869593806060025.

Li, Z.X., Zhang, L., and Powell, C.M., 1996, Positions of the East Asian cratons in the Neoproterozoic supercontinent Rodinia: Australian Journal of Earth Sciences, v. 43, p. 593–604, doi: 10.1080/08120099608728281.

Liu, Y., Gao, L., Liu, Y., Song, B., and Wang, Z., 2006, Zircon U-Pb dating for the earliest Neoproterozoic mafic magmatism in the southern margin of the North China Block: Chinese Science Bulletin, v. 51, p. 2375–2382, doi: 10.1007/s11434-006-2114-0.

Liu, F., Zhang, J., and Liu, C., 2017, Archean to Paleoproterozoic Evolution of the North China Craton : Preface: Precambrian Research, v. 303, p. 1–9, doi: 10.1016/j.precamres.2017.11.011.

McArthur, J.M., Howarth, R.J., and Shields, G.A., 2012, Strontium Isotope Stratigraphy: The

Geologic Time Scale, p. 127–144, doi: 10.1016/B978-0-444-59425-9.00007-X.

Melezhik, V.A., Ihlen, P.M., Kuznetsov, A.B., Gjelle, S., Solli, A., Gorokhov, I.M., Fallick, A.E., Sandstad, J.S., and Bjerkgård, T., 2015, Pre-Sturtian (800-730Ma) depositional age of carbonates in sedimentary sequences hosting stratiform iron ores in the Uppermost Allochthon of the Norwegian Caledonides: A chemostratigraphic approach: Precambrian Research, v. 261, p. 272–299, doi: 10.1016/j.precamres.2015.02.015.

Melezhik, V.A., Pokrovsky, B.G., Fallick, A.E., Kuznetsov, A.B., and Bujakaite, M.I., 2009, Constraints on $^{87}Sr/^{86}Sr$ of Late Ediacaran seawater: insight from Siberian high-Sr limestones: Journal of the Geological Society, v. 166, p. 183–191, doi: 10.1144/0016-76492007-171.

Mii, H., Grossman, E.L., Yancey, T.E., Horng-sheng, M.E.L.G.T.E.Y., Mii, H., Grossman, E.L., and Yancey, T.E., 1997, Stable carbon and oxygen isotope shifts in Permian seas of West Spitsbergen-Global change or diagenetic artifact? Geology, v. 25, p. 225–227, doi: 10.1130/0091-7613(1997)025<0227.

Misi, A., and Veizer, J., 1998, Neoproterozoic carbonate sequences of the Una Group, Irece Basin, Brazil: Chemiostratigraphy, age and correlations: Precambrian Research, v. 89, p. 87–100.

Montanez, I.P., Banner, J.L., Osleger, D.A., Borg, L.E., and Bosserman, P.J., 1996, Integrated Sr isotope variations and sea-level history of middle to Upper Cambrian platform carbonates: Implications for the evolution of Cambrian seawater $^{87}Sr/^{86}Sr$: Geology, v. 24, p. 917–920, doi: 10.1130/0091-7613(1996)024<0917:ISIVAS>2.3.CO.

Peng, P., Bleeker, W., Ernst, R.E., Söderlund, U., and McNicoll, V., 2011, U–Pb baddeleyite ages, distribution and geochemistry of 925Ma mafic dykes and 900Ma sills in the North

China craton: Evidence for a Neoproterozoic mantle plume: Lithos, v. 127, p. 210–221, doi: 10.1016/j.lithos.2011.08.018.

Pokrovskii, B.G., Melezhik, V. a., and Bujakaite, M.I., 2006, Carbon, oxygen, strontium, and sulfur isotopic compositions in late Precambrian rocks of the Patom Complex, central Siberia: Communication 2. Nature of carbonates with ultralow and ultrahigh δ13C values: Lithology and Mineral Resources, v. 41, p. 576–587, doi: 10.1134/S002449020606006X.

Pollock, M.D., Kah, L.C., and Bartley, J.K., 2006, Morphology of Molar-Tooth Structures in Precambrian Carbonates: Influence of Substrate Rheology and Implications for Genesis: Journal of Sedimentary Research, v. 76, p. 310–323, doi: 10.2110/jsr.2006.021.

Pope, M.C., Bartley, J.K., Knoll, A.H., and Petrov, P.Y., 2003, Molar tooth structures in calcareous nodules, early Neoproterozoic Burovaya Formation, Turukhansk region, Siberia: Sedimentary Geology, v. 158, p. 235–248, doi: 10.1016/S0037-0738(02)00312-3.

Rooney, A.D., Macdonald, F. a, Strauss, J. V, Dudás, F.Ö., Hallmann, C., and Selby, D., 2014, Re-Os geochronology and coupled Os-Sr isotope constraints on the Sturtian snowball Earth.: Proceedings of the National Academy of Sciences of the United States of America, v. 111, p. 51–6, doi: 10.1073/pnas.1317266110.

Shen, B., Dong, L., Xiao, S., Lang, X., Huang, K., Peng, Y., and Zhou, C., 2016, Molar tooth carbonates and benthic methane fluxes in Proterozoic oceans: Nature Communications, v. 7, p. 1–6, doi: 10.1038/ncomms10317.

Shields, G.A., 2002, “Molar-tooth microspar”: a chemical explanation for its disappearance ~ 750Ma: Terra Nova, v. 14, p. 108–113.

Shields, G.A., 1999, Working towards a new stratigraphic calibration scheme for the Neoproterozoic-Cambrian: ECLOGAE GEOLOGICAE HELVETIAE, v. 92, p. 221–233.

Tang, Q., Pang, K., Xiao, S., Yuan, X., Ou, Z., and Wan, B., 2013, Organic-walled microfossils from the early Neoproterozoic Liulaobei Formation in the Huainan region of North China and their biostratigraphic significance: Precambrian Research, v. 236, p. 157–181, doi: 10.1016/j.precamres.2013.07.019.

Tang, Q., Pang, K., Yuan, X., Wan, B., and Xiao, S., 2015, Organic-walled microfossils from the Tonian Gouhou Formation, Huaibei region, North China Craton, and their biostratigraphic implications: Precambrian Research, v. 266, p. 296–318, doi: http://dx.doi.org/10.1016/j.precamres.2015.05.025.

Veizer, J., 1983, CHAPTER 3 CHEMICAL DIAGENESIS OF CARBONATES : THEORY AND APPLICATION OF, *in* Stable Isotopes in Sedimentary Geology, v. SC10, p. 3-1-3–99.

Wan, B., Tang, Q., Pang, K., Wang, X., Bao, Z., and Meng, F., 2019, Repositioning the Great Unconformity at the southeastern margin of the North China Craton: Precambrian Research, v. 324, p. 1–17, doi: 10.1016/j.precamres.2019.01.014.

Wang, H., and Qiao, X., 1984, Proterozoic stratigraphy and tectonic framework of China: Geological Magazine, v. 121, p. 599–614, doi: 10.1017/S0016756800030740.

Wang, Q.H., Yang, D. Bin, and Xu, W.L., 2012, Neoproterozoic basic magmatism in the southeast margin of North China Craton: Evidence from whole-rock geochemistry, U-Pb and Hf isotopic study of zircons from diabase swarms in the Xuzhou-Huaibei area of China: Science China Earth Sciences, v. 55, p. 1461–1479, doi: 10.1007/s11430-011-4237-7.

Wang, W., Zhou, M.F., Yan, D.P., and Li, J.W., 2012, Depositional age, provenance, and tectonic setting of the Neoproterozoic Sibao Group, southeastern Yangtze Block, South China: Precambrian Research, v. 192–195, p. 107–124, doi:

10.1016/j.precamres.2011.10.010.

Xiao, S., Shen, B., Tang, Q., Kaufman, A.J., Yuan, X., Li, J., and Qian, M., 2014, Biostratigraphic and chemostratigraphic constraints on the age of early Neoproterozoic carbonate successions in North China: Precambrian Research, v. 246, p. 208–225, doi: 10.1016/j.precamres.2014.03.004.

Yang, D. Bin, Xu, W.L., Xu, Y.G., Wang, Q.H., Pei, F.P., and Wang, F., 2012, U-Pb ages and Hf isotope data from detrital zircons in the Neoproterozoic sandstones of northern Jiangsu and southern Liaoning Provinces, China: Implications for the Late Precambrian evolution of the southeastern North China Craton: Precambrian Research, v. 216–219, p. 162–176, doi: 10.1016/j.precamres.2012.07.002.

Yang, J., Zheng, W., Wang, Z., and Tao, X., 2001, Age determining of the uppe Precambrian system of Northern Jiangsu-Anhui by using Sr and C isotopes: Journal of Statigraphy (in Chinese), v. 25, p. 44–47.

Yoshioka, H., Asahara, Y., Tojo, B., and Kawakami, S. ichi, 2003, Systematic variations in C, O, and Sr isotopes and elemental concentrations in neoproterozoic carbonates in Namibia: Implications for a glacial to interglacial transition: Precambrian Research, v. 124, p. 69–85, doi: 10.1016/S0301-9268(03)00079-2.

Zang, W.-L., and Walter, M.R., 1992, Late Proterozoic and Early Cambrian microfossils and biostratiraphy, Northern Anhui and Jiangsu: Precambrian Research, v. 57, p. 243–323.

Zhang, S., Li, Z.-X., Wu, H., and Wang, H., 2000, New paleomagnetic results from the Neoproterozoic successions in southern North China Block and paleogeographic implications: Science in China Series D: Earth Sciences, v. 43, p. 233–244, doi: 10.1007/BF02911948.

Zhang, S., Zhao, Y., Ye, H., and Hu, G.H., 2016, Early Neoproterozoic emplacement of the diabase sill swarms in the Liaodong Peninsula and pre-magmatic uplift of the southeastern North China Craton: Precambrian Research, v. 272, p. 203–225, doi: 10.1016/j.precamres.2015.11.005.

Zhao, G., and Guo, J., 2012, Precambrian geology of China: Preface: Precambrian Research, v. 222–223, p. 1–12, doi: 10.1016/j.precamres.2012.09.018.

Zhao, G., Sun, M., Wilde, S.A., and Sanzhong, L., 2005, Late Archean to Paleoproterozoic evolution of the North China Craton: Key issues revisited: Precambrian Research, v. 136, p. 177–202, doi: 10.1016/j.precamres.2004.10.002.

Zheng, W., Yang, J., Hong, T., Tao, X., and Wang, Z., 2004, Sr and C Isotopic Correlation and the Age Boundary Determination for the Neoproterozoic in the Southern Liaoning and Northern Jiangsu Northern Anhui Provinces: Geological Journal of China Universit ies (in Chinese), v. 10.

Zhu, R., Ni, P., Wang, G., Ding, J., Fan, M., and Ma, Y., 2019, Geochronology , geochemistry and petrogenesis of the Laozhaishan dolerite sills in the southeastern margin of the North China Craton and their geological implication: Gondwana Research, v. 67, p. 131–146, doi: 10.1016/j.gr.2018.10.016.